ACS APPLIED MATERIALS & INTERFACES

www.acsami.org

Research Article

Oil-Membrane Protection of Electrochemical Sensors for Fouling- and pH-Insensitive Detection of Lipophilic Analytes

Yuchan Yuan, Madeleine DeBrosse, Michael Brothers, Steve Kim, Alexandra Sereda, Nikolai V. Ivanov, Saber Hussain, and Jason Heikenfeld*

Cite This: https://doi.org/10.1021/acsami.1c14175

Read Online

ACCESS | Metrics & More | Article Recommendations | Supporting Information

ABSTRACT: To take full advantage of the reagent- and label-free sensing capabilities of electrochemical sensors, a frequent and remaining challenge is interference and degradation of the sensors due to uncontrolled pH or salinity in the sample solution or foulants from the sample solution. Here, we present an oil-membrane sensor protection technique that allows for the permeation of hydrophobic (lipophilic) analytes into a sealed sensor compartment containing ideal salinity and pH conditions while simultaneously blocking common hydrophilic interferents (proteins, acids, bases, etc.) In this paper, we validate the oil-membrane sensor protection technique by demonstrating continuous cortisol detection via electrochemical aptamer-based (EAB) sensors. The encapsulated EAB cortisol sensor exhibits a 5 min concentration-on rise time and maintains a measurement signal of at least 7 h even in the extreme condition of an acidic solution of pH 3.

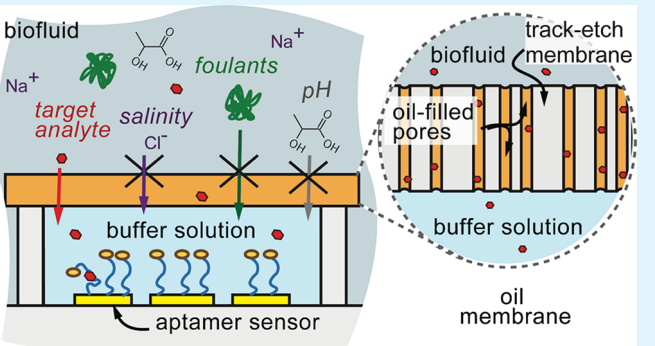

KEYWORDS: *electrochemical aptamer-based sensor, oil membrane, pH independent, anti-fouling*

INTRODUCTION

Enzymatic sensors are most commonly deployed for both real-time[1] and point-of-care assays because of the ability to couple a biochemical reaction to a change in redox state of a co-factor (e.g., NADH and FADH2) that can be measured directly or indirectly.[2] However, enzymatic sensors are particularly sensitive to changes in pH and salinity, as they are composed of amino acids. Enzymes, as well as other proteins, are inherently pH-sensitive because of their labile side-chain protonation sites and salinity-sensitive because of their charged functional groups.[5] Therefore, any change in salinity and/or pH must be accounted for with regard to converting enzymatic activity to analyte concentration.

Other biosensors that utilize biorecognition elements suffer from similar constraints, including electrochemical aptamer-based (EAB) sensors invented by Plaxco and colleagues.[6] These sensors rely on the high binding affinity of the analyte to the aptamer. Aptamers are known to be sensitive to both salinity and pH,[4,7] thus impacting the sensor performance and analyte response. Additionally, EAB sensors use an immobilized methylene blue redox couple, which itself is highly pH-sensitive.[8]

Up until recently, electrochemical sensor demonstrations have been dominantly performed in buffer fluids, sera, or blood because these fluids are highly relevant testing standards. All of these fluids are well-buffered regarding their pH and salinity, which would otherwise confound sensor response.[3,4] Unlike blood or buffer solutions, pH and salinity changes can be particularly acute for continuous sensing in emergent applications such as sweat biomarkers[3] and of environmental pollution, in both of which pH and salinity can be highly variable. Even in a well-buffered biofluid such as blood, there are also some ranges of pH and specific salts such as $MgCl_2$ that produce maximum performance for enzymes[9] or aptamers,[10] and therefore, local control of pH and salinity at the sensor can be desirable.

With specific respect to biofluids, the majority of the most problematic solutes are hydrophilic, including salts, acids, bases, and larger molecules such as proteins, which must have a hydrophilic shell to maintain their water solubility. Generalizing the problematic solutes as hydrophilic presents a significant opportunity for more robust sensing of hydrophobic solutes since hydrophilic/hydrophobic selective protection could theoretically be added to sensors. Implementing such a hydrophilic/hydrophobic filter would provide protection even

Received: July 28, 2021
Accepted: October 7, 2021

beyond the widely deployed size-selective protective membranes such as those used for in vivo glucose sensors[11−13] and other EAB sensors.[14] Furthermore, this membrane should filter out redox-active interfering agents such as the negatively charged FAD/FADH2 and NAD+/NADH coenzymes.

In response to this opportunity, we present here a novel approach of oil-membrane sensor protection, which allows for the permeation of hydrophobic (lipophilic) analytes into a sealed compartment containing the sensor in its ideal pH condition, while the same oil membrane simultaneously blocks protein foulants and pH interferents (acids/bases). In this paper, we specifically validate an oil-membrane sensor protection technique by demonstrating continuous cortisol detection via EAB sensors. The oil-membrane encapsulated EAB cortisol sensor exhibits a 5-min concentration-on rise time and a measurement signal over at least 7 h even under an extremely acidic condition of pH 3. This paper presents both the sophistication of oil-membrane physics and the resulting design criteria. Limitations and proposed improvements of our current approach and novel methods for rapidly optimizing the oil-membrane technique for new analytes and applications are also discussed.

From an application perspective, the novel oil-membrane approach presented here is important for numerous applications, including those with hydrophobic analytes, such as orally administered drugs (hydrophobic by design for gut permeation), and steroid hormones (cortisol, testosterone, estrogen, melatonin, etc.). Improved robustness to variable pH also satisfies an acute and immediate need for sweat biosensing, where pH can vary significantly.[3,15] On a speculative level, as biosensing researchers look toward implanted biosensors, having sensor protection even more robust than size-selective membranes could certainly be valuable, especially if the sensor is preserved in optimal buffer conditions. In addition, oil-membrane protection may prove important as biosensing moves into areas that require alternative fluids with non-ideal pH and salinity, such as environmental sensing or food processing.[16] Many emerging potent biotoxins are hydrophobic because of the need to rapidly permeate biological tissue and therefore are ideal candidates for oil-membrane protection.[17] Lastly, oil-membrane protection may also prove important because many hydrophobic analytes in biofluids tend to bind to transport proteins, such as albumin,[15] thus greatly reducing the unbound drug concentration for detection by electrochemical sensors. Oil-membrane protection could allow for protein denaturation by using salts or pH outside the membrane barrier to release the hydrophobic analytes such that they are increased to measurable concentrations while still preserving the sensor environment. Simply, oil-membrane sensor protection has the potential to open up numerous biosensing applications that are currently challenged or even unobtainable with electrochemical sensors.

THEORETICAL BASIS AND DEVICE DESIGN

EAB Sensor for Cortisol Sensing. This manuscript relies on an unpublished EAB sensor for cortisol to simply validate the oil-membrane technique (cortisol aptamer provided by Eccrine Systems Inc.) and is not intended to be about the application of cortisol sensing. EAB sensors are affinity-based biosensors that equilibrate their signal to the analyte concentration.[8] For the EAB sensors (Figure 1b,c), aptamers (oligonucleotides) are immobilized on a gold working

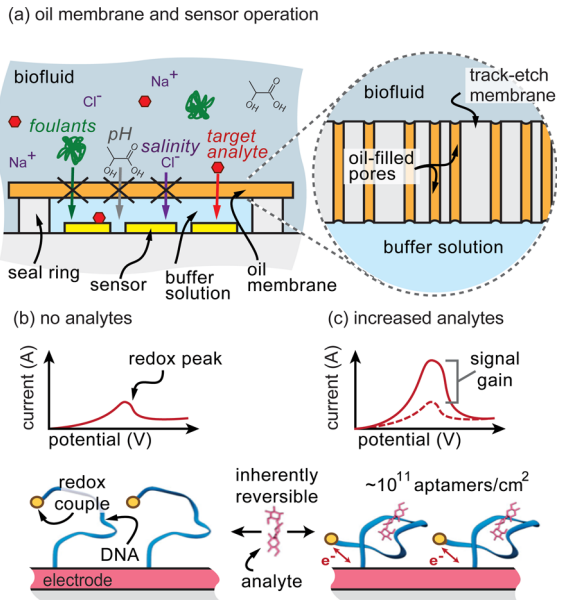

Figure 1. (a) The oil membrane allows the partitioning of hydrophobic analytes such as cortisol while blocking hydrophilic solutes such as proteins, salts, and acids/bases. (b) For the electrochemical aptamer-based (EAB) sensors used in this work, a gold working electrode is functionalized with DNA aptamers terminated with a redox couple. (c) The aptamers fold with the presence of the target analyte, which changes the proximity of the redox couple with the electrode compared to (b) without the target analyte, resulting in a change in electrical current that correlates with the change in analyte concentration.

electrode using thiol-linkers. Opposite to its thiol end, the aptamer is tagged with a methylene-blue redox reporter. Figure 1b shows the functionalized working electrode in the "off" position, where the redox couple is extended away from the gold surface when the aptamer sits in its unfolded or partially unfolded state. Upon analyte binding, shown in Figure 1c, the aptamer folds in on itself, changing the redox-couple distance from the electrode surface. This activity alters the electron transfer rate from the redox couple to the working electrode, resulting in a change in electrical current measured by square-wave voltammetry.

Comparing the current before and after binding of the analyte, a signal gain can be calculated, which is proportional to the change in the target analyte concentration. Previous studies have shown that pH and salinity have a substantial impact both on the binding affinity between the analyte and aptamer and on the current generated by the pH-sensitive redox reporter.[8] For this reason, the EAB sensor is an excellent platform to test the performance of an oil membrane for sensor protection.

Adding Oil-Membrane Protection onto the EAB Sensor. The oil-membrane encapsulation strategy (Figure 1a) involves an oil-impregnated hydrophobic membrane that provides a barrier between the sensing compartment and the test fluids, thereby blocking interferents and improving sensor performance. The oil membrane is designed to provide a constant, stable hydrophobic barrier that allows the simultaneous permeation of hydrophobic analytes, such as cortisol molecules, while maintaining ideal aqueous conditions at the sensor side, such as salinity and pH.

Figure 2 contains more detailed diagrams of the specific oil-membrane protected EAB cortisol sensors used in this paper. This sensor uses a three-electrode system. Four working

https://doi.org/10.1021/acsami.1c14175
ACS Appl. Mater. Interfaces XXXX, XXX, XXX−XXX

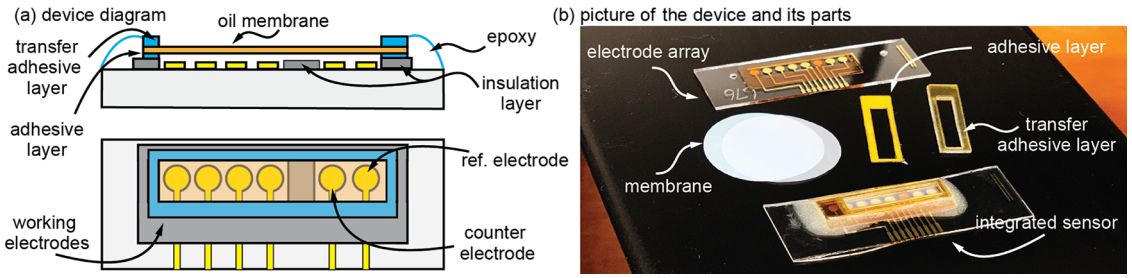

Figure 2. (a) Diagram of side/top view of the oil-membrane sealed EAB cortisol sensor. (b) Picture of the oil-membrane sealed EAB cortisol sensor and its parts both before and after assembly.

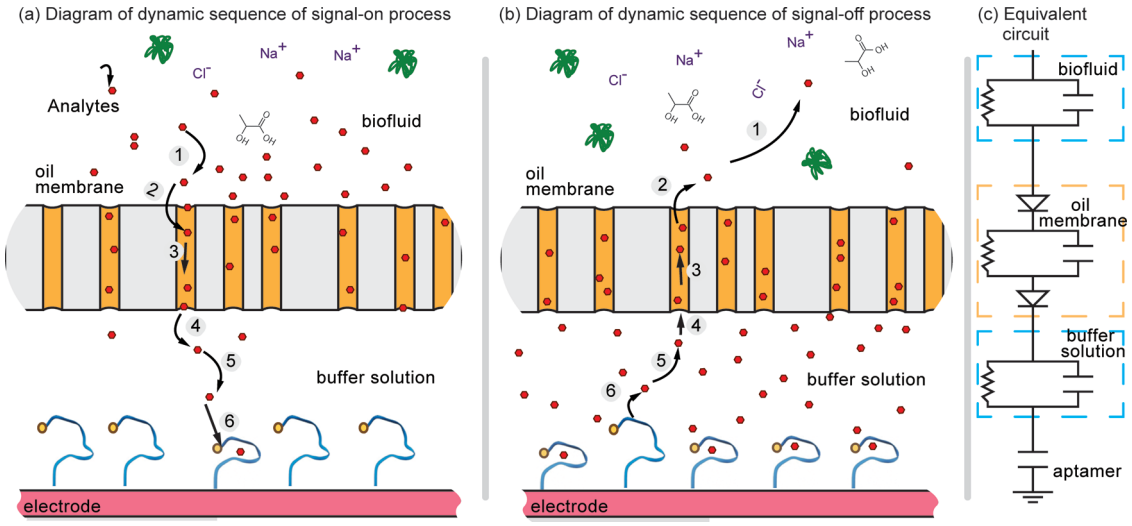

Figure 3. (a) During the concentration-on process, the hydrophobic analyte molecule (1) diffuses to the interface between the oil membrane and biofluid and (2) rapidly partitions into the oil (decrease in free energy). (3) The analyte diffuses to the other end of the oil membrane, (4) more slowly partitions out of oil with a lag time (increase in free energy), and (5) diffuses close to the sensor surface. (6) The analyte binds with the aptamer. (b) The reverse process. (c) A simple circuit representation of the system is provided as an additional guide, and it should be noted that it is an approximation and not a theoretically equivalent model.

electrodes share one common counter electrode and one pseudo-reference electrode. Gold is used for the surface of all electrodes; however, only the working electrodes feature the EAB sensor functionalization with the aptamer and redox couple. After the EAB sensors are fabricated, a layer of Kapton polyimide film is applied as a chemical and electrical insulation layer. Next, the oil membrane is sandwiched along its perimeter between two layers of adhesive and fixed to the Kapton/substrate. The placement of the oil membrane onto the Kapton/substrate is performed while this device is submerged in a bath of buffer solution such that the buffer solution is sealed inside the device. Lastly, the edges of the oil membrane are further sealed against the Kapton/substrate by applying marine epoxy to improve the robustness of the seal. Figure 2b shows a picture of a fully integrated device and its individual components. A more detailed material list and fabrication process is included in the Methods section.

Physics behind Oil-Membrane Operation and Resulting Design. The permeability of the oil membrane affects sensor response time and is the first design element we will discuss in detail. An oil membrane will slow down the permeability (diffusion) of analytes to the sensor according to eq 1:[18]

$$P = \frac{K \times D}{z}\left(\frac{\text{cm}}{\text{s}}\right) \quad (1)$$

where the partition coefficient (K) is defined as the ratio of the concentrations at equilibrium of the analyte molecules in the oil vs in the water, D is the diffusion coefficient for the analyte in the oil, and z is the thickness of the oil layer. Equation 1 is informative to the oil-membrane design but can also be misleading. We will first discuss how eq 1 is informative.

The permeability equation (eq 1) clearly shows that a thinner membrane and, therefore, thinner oil thickness (z) will increase the membrane permeability (P). For this reason, we chose 11 μm thick polycarbonate track-etch membranes instead of thicker hydrophobic membranes such as conventional porous Teflon films (z = 10s to 100s of μm). The oil wicks into and remains in the track-etch membrane pores because of its lower interfacial surface tension with the polycarbonate than the water has with polycarbonate. The membrane permeability equation (eq 1) also clearly reveals that a high diffusion coefficient D matters as well. The diffusion coefficient of an analyte is dependent on the viscosity of the fluid it is diffusing through. Therefore, an important design element for the oil is to have a low viscosity (diffusion coefficient is inversely proportional to the viscosity of the oil[18]). Consider an informative example related to the materials used here. The optimal track-etch membranes for this work (see Table S1) have an 11 μm membrane thickness and 15.7% porosity, which are equivalent to the analyte having to diffuse through a uniform 70 μm of oil (11 μm/0.157).

https://doi.org/10.1021/acsami.1c14175
ACS Appl. Mater. Interfaces XXXX, XXX, XXX−XXX

Table 1. Selected Oils that Were Initially Screened along with Their Relevant Properties[a]

	melting point (°C)	LogK (water over octanol)	viscosity at 25 °C (cP)	vapor pressure at 25 °C (mmHg)	solubility in water (mg/L)	carbon #	double bonds (in chain)	structural family
tetradecane	6	8.19	2.13	0.0369	0.00033	14	0	saturated hydrocarbon
castor oil	−10 to −12	17.72	650	<0.097	<0.001	57	3	trigyceride mixture
1-decanol	6.67	4.57	12	0.00851	30	10	0	fatty alcohol
dioctyl ether	−7.6	6.9	0.224	0.005		16	0	dialkyl ether
oleic acid	16.3	7.64	27.64	0.0000005	0.01	18	1	unsaturated fatty acid
vitamin K1	−20	10.9				31	1	polycyclic aromatic ketone
mineral oil				<0.1				
dodecane thiol	−7 to −9	6.1		0.000015	<0.2	12	0	alkyl thiol

[a]LogK is the logarithm of the ratio of molecule concentration of the oil in octanol and water at equilibrium.[21−27]

Consider castor oil, with a viscosity about 730 times greater than that of water (see Table S2). An 11 μm thick castor oil membrane would then be equivalent to a 51,170 μm thick water diffusion distance (11 μm/0.157 × 730). Alternatively, using a low-viscosity oil, such as 1-decanol, the 11 μm thick oil membrane would have an equivalent thickness of only 945 μm diffusion distance through water (see Table S2).

We have saved the oil/water partition coefficient K for the last part of our discussion. Although eq 1 suggests that a high K is advantageous, it is actually misleading. In a static case, where concentration gradients are held constant on both sides of the oil membrane and the analyte is constantly diffusing through a membrane, eq 1 states that the highest possible K is beneficial. However, a very high K can be problematic in dynamic cases. An EAB sensor has to dynamically equilibrate to an often-changing analyte concentration in the biofluid; therefore, it is more important to understand the specific impact of a high K with rising or falling analyte concentrations on the biofluid side of the oil membrane. Figure 3 illustrates the dynamic case for the concentration-on and -off process; we will describe this in detail and then explain why a high K is problematic.

When the cortisol concentration increases on the biofluid side, the analyte first diffuses to the interface between the biofluid and the oil membrane (Figure 3a, 1). It then partitions into the oil (Figure 3a, 2) followed by its diffusion to the other end of the oil pore inside the membrane (Figure 3a, 3). Due to their hydrophobic nature, analytes such as cortisol energetically prefer to remain in the oil (lower free energy),[19,20] and additional retention time can occur as the analyte attempts to leave the oil and partition into the water by the sensor (Figure 3a, 4). Afterward, analytes diffuse closer to the sensor surface (Figure 3a, 5) and bind with the aptamer when the analyte concentration nears the binding affinity of the aptamer (Figure 3a, 6). As shown in Figure 3b, the entire process is reversible.

A high K is problematic for two reasons. First, the oil can become a huge sink for the analyte. Consider a K value of 10,000 using our 11 μm track-etch membrane with 15.7% porosity. With the concentration of the analyte in the oil being 10,000 times higher than that in the water, the "effective volume" of the oil in terms of analyte capacity is equivalent to 11 μM × 0.157 ×10,000 = 17.27 cm of water. Clearly, K cannot be too large for this reason. A second reason why a high K is problematic is the oil retention of the analyte (lower free energy in the oil than in the water). A higher K can cause the oil to retain the analyte and induce an additional lag time as the analyte attempts to leave the oil and partition back into water. For the concentration-on process, this oil-to-water lag time is not a major concern for the device because the volume of the buffer solution is small, which reduces the total amount of analyte that must partition into the buffer solution (short lag time). For the concentration-off process, however, it is difficult for the analyte concentration in the buffer solution to decrease quickly because the analyte concentration in the oil must first decrease, which is limited by the high K value of the oil (inherently a very high concentration of the analyte). Therefore, the oil-to-water lag time as the analyte goes from the oil back into the biofluid can create a major bottleneck for the concentration-off process because the oil has acquired such a high concentration of the analyte. This much slower concentration-off response time will be observable later in the experimental results.

Although our discussion on the oil-membrane physics remains focused on analyte transport, it also affects the device design for blocking foulants and interferents. K will always have some finite value even for hydrophilic acids, bases, and salts (it is never zero), and K depends on the charge state of the solute, which can further depend on the pH of the biofluid (solute ionization constants pKa and pKb). For example, a solute might be found primarily in its charged state (98%) within a biofluid of a specific pH. The remaining 2% remains in an uncharged state and may diffuse through the protective oil-membrane barrier. For this reason, it is important to understand the effects of pH on analyte properties. Therefore, as the experimental data will show, the oil membrane provides a limited protection over time.

Lastly, the oil viscosity and oil partition coefficient (K) are not the only relevant materials parameters for oil optimization (Table 1). For most sensor applications, the oil must remain liquid at room temperature while also having low vapor pressure such that it is not rapidly lost during assembly or potential dry storage. The solubility of the oil in water is also critical because eventual oil loss into water could cause failure in the oil-membrane protection of the sensor. A simple example calculation is as follows. Consider a device that is brought into contact with 0.3 μL of biofluid per minute and a sensor and membrane area of 0.1 cm^2 with the membrane containing 0.0173 μL of oil. Assuming that all the oil that could partition into the water does so at any given time (an unrealistic but instructive assumption), if the device were to operate continuously for 24 h without losing all the oil to the biofluid, the water solubility of the oil would need to be less than 36 mg/L.

https://doi.org/10.1021/acsami.1c14175
ACS Appl. Mater. Interfaces XXXX, XXX, XXX−XXX

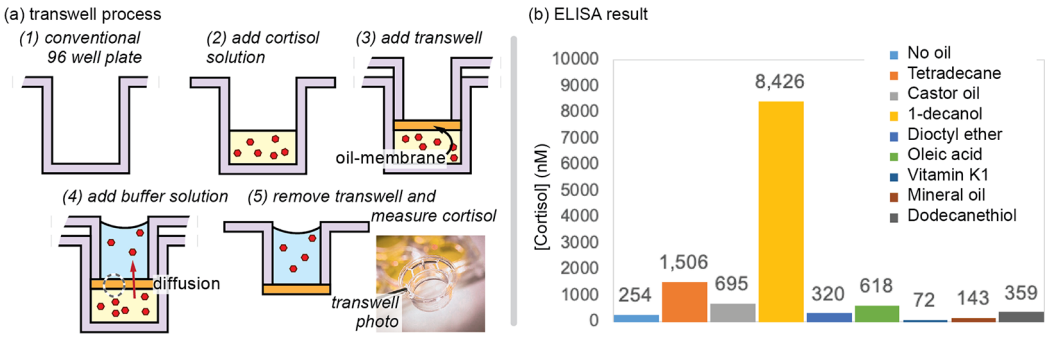

Figure 4. (a) Transwell setup steps for characterizing cortisol partitioning through different oils. (b) ELISA results of cortisol diffusing through selected oils in the upper well solution after 2 h of incubation at room temperature.

EXPERIMENTS AND RESULTS

Initial Oil Screening Test. As noted in the Theoretical Basis and Device Design section, oil choice is a critical element for the successful realization of the oil-membrane technique. The nine different oils listed in Table 1 are initially selected and tested. Initial selection parameters are based on low water solubility and low vapor pressure to ensure long-term oil integrity within the membrane pores. In addition, oils with positive octanol/water K values are favored because of the hydrophobic nature of the test analyte (cortisol) while achieving a low permeability for hydrophilic interferents (pH and salinity).

To rapidly screen the oil candidates, a commercially available transwell setup is modified to measure the concentration of diffused cortisol through transwell membranes with different oils. Figure 4a shows a diagram of the experimental process. First, the bottom well is filled with 235 μL of 1× phosphate-buffered saline (PBS) solution with a cortisol concentration of 10 μM (Figure 4a, 1–2). The traditional transwell membrane of the upper well is removed and replaced with a hydrophobic polycarbonate track-etch membrane used throughout this work (11 μm thick, 15.7% porosity, and 1 μm diameter pore size). Each oil is applied to individual track-etch membrane, and the upper transwell is placed into the bottom wells (Figure 4a, 3). Then, as shown in Figure 4a, 4, the upper transwell is filled with 180 μL of cortisol-free 1× PBS solution. The 96-well plate is then covered and incubated for 2 h at room temperature to allow the cortisol to diffuse from the bottom well to the upper well through the oil-soaked membrane. The solution in the upper well is collected for analysis (Figure 4a, 5) using commercially available ELISA kits.

Figure 4b displays the ELISA cortisol concentration results obtained by different oil membranes. The solution from the 1-decanol membrane sample contains the most cortisol—more than 5× the cortisol concentration of the second-ranking tetradecane membrane. The third-ranking membrane, castor oil, possesses less than half of the cortisol concentration of the tetradecane membrane. Castor oil is known to be an excellent oil for dissolving drugs and steroid hormones[28,29] and therefore likely possesses a very high K for cortisol. Also, the high viscosity of the castor oil should slow the diffusion of the cortisol through the oil (eq 1), leading to a lower cortisol concentration for castor oil than that for the lower-viscosity 1-decanol.[30]

Directly Testing Oils against pH, Salt, and Protein Permeability. Before testing the integrated devices, the top three performing oils (1-decanol, tetradecane, and castor oil) are tested directly against a high salt solution and extreme acidic solution. A U-boat setup is employed to measure salt diffusion from one buffer solution compartment to another separated by an oil membrane (Figure 5a). For the salt diffusion test, a 10 mL buffer solution containing 150 mM NaCl is placed in the right (control) chamber and 10 mL of distilled (DI) water is placed in the left (monitored) chamber. The two chambers are separated by an oil-impregnated membrane secured by two rubber washers. The electrical resistance of the solution is measured in 60 s increments using a CHI 600E potentiostat, as shown in Figure 5b. A similar setup (see Methods) is used for the pH diffusion test. For this test, a 10 mL solution at pH 3 is placed in the control (right) chamber and 10 mL of DI water is placed in the monitor (left) chamber. The pH value of the monitored solution is measured in 60 s increments using an Orion Star benchtop pH meter (Thermo Fisher Scientific Inc., Waltham, MA), as shown in Figure 5c. Test results with highly alkaline solution are not presented here since our initial focus is on the application of oil membrane in

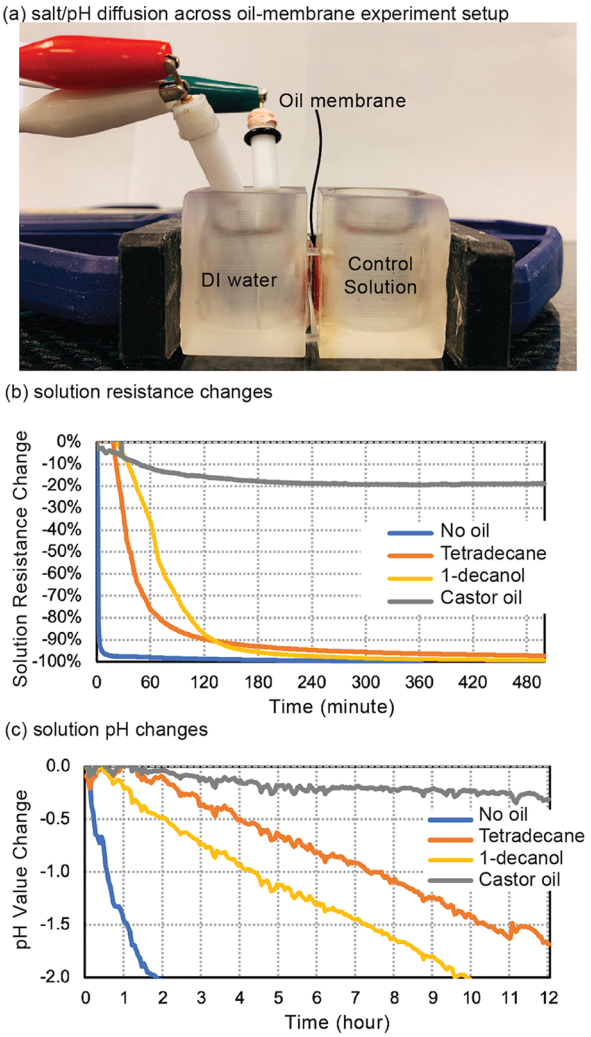

Figure 5. (a) Experiment setup for the salt/pH diffusion test with different oils. (b, c) Electrical resistance and chemical pH changes over time. The same test setup as in (a) is used. Extreme cases of pH = 3 and 150 mM/0 mM salt were used.

https://doi.org/10.1021/acsami.1c14175
ACS Appl. Mater. Interfaces XXXX, XXX, XXX−XXX

biofluids such as sweat and saliva whose pH ranges from 4.5 to 7.5.[3,31,32]

As shown in Figure 5b,c, castor oil shows the best performance in terms of blocking interfering species, tetradecane the second, and then 1-decanol the least. The castor-oil-saturated membrane maintains the pH within half a unit change over 12 h. Within 8 h, the tetradecane-saturated membrane can maintain pH changes within one unit. However, 1-decanol fails to maintain the pH within two unit changes after 10 h. Although it is expected that acids and bases might diffuse through an oil, surprisingly, simple salts such as NaCl diffuse through as well under our extreme initial test conditions (150 mM/0 mM). This becomes less surprising when considering that the octanol/water LogK for Cl− is 0.06 and that for Na+ is −0.77 (low but adequate to permit diffusion through the oil). Fortunately, for the cortisol aptamer sensor demonstrated in this paper, salinity change does not negatively influence the sensor performance. The salinity test (see Figure S1) shows that a higher salt concentration increases the signal current magnitude and to some level increases the absolute signal gain on the target concentration. In the future, we speculate that by choosing and/or blending different oils, we can likely further increase the resistance of the oil membrane to salt diffusion, and in real applications, the salinity differences can easily be designed to be smaller across the membrane (not our extreme case of 150 mM/0 mM). Furthermore, as we will discuss in the next sections, devices were demonstrated as stable with very high salt conditions in the sensor buffer solution (33× buffer, Figure S2) and as stable with continuous salt mitigation (Figure 8). Lastly, to confirm that the oil membrane effectively blocks protein interferents, we tested oil-membrane protection and exposed it to serum for >12 h (Figure S8) and observed a fairly stable sensor operation in terms of electron transfer at the working electrode but some fouling likely due to small hydrophobic solutes in the serum (small changes in electrode impedance). With the results of Figures 4 and 5, tetradecane, 1-decanol, and castor oil are advanced to the next phase of experimentation with integrated aptamer sensors for cortisol.

Initial Sensor Tests as Control Experiments. The sensors are first characterized directly for the effects of pH on sensor response to aid in the interpretation of EAB sensor data. To initially find the optimal pH environment for the specific cortisol-binding aptamer used in this paper, a three-electrode system is tested: an aptamer-functionalized gold disk electrode, a Pt wire counter electrode, and a Ag/AgCl reference electrode. The sensor system is tested for 5 min in each solution—with and without cortisol—to measure the on/off signal performance. The pH of the sensor solution is varied from pH 8.5 to 5.5. The activity of methylene blue is demonstrated by the signal gain as a function of time pre- and post-cortisol exposure (Figure 6a). The highest signal gain is observed at pH 7.5. As the solution becomes more acidic, the signal gain decreases, and the redox peak shifts toward a more positive potential. As an additional control experiment to further reveal the negative impact of pH and the positive impact of oil-membrane protection, another U-boat test setup in a similar manner to Figure 5a is implemented but using a cortisol EAB sensor to monitor sensor functionality. The monitor side is filled with 10 mL of synthetic sweat solution (SSS) at pH 7.5 without cortisol, while the control side is filled with SSS containing a 10 μM cortisol concentration at pH 3. Castor oil is used as the oil in the oil membrane. As shown in Figure 6b, the sensor with the oil-membrane protection responds to cortisol by an increase in redox-couple peak current, and the redox-couple peak position (potential) remains stable over time. Conversely, the same experiment but without oil in the membrane (water-filled) shows in Figure 6c that the signal gain response decreases and the redox peak rapidly shifts in potential. With these promising results in hand, the next set of experiments pursues the testing of fully integrated devices.

Fully Integrated Device Tests. For the remainder of experiments, fully integrated devices are tested using components previously illustrated in Figure 2. SSS at pH 7.5 is again used as the solution on the sensor side of the oil membrane. For the "biofluid" side of the oil membrane, the bulk solution is varied in pH (pH 3 or 7.5) and cortisol content (0 or 10 μM).

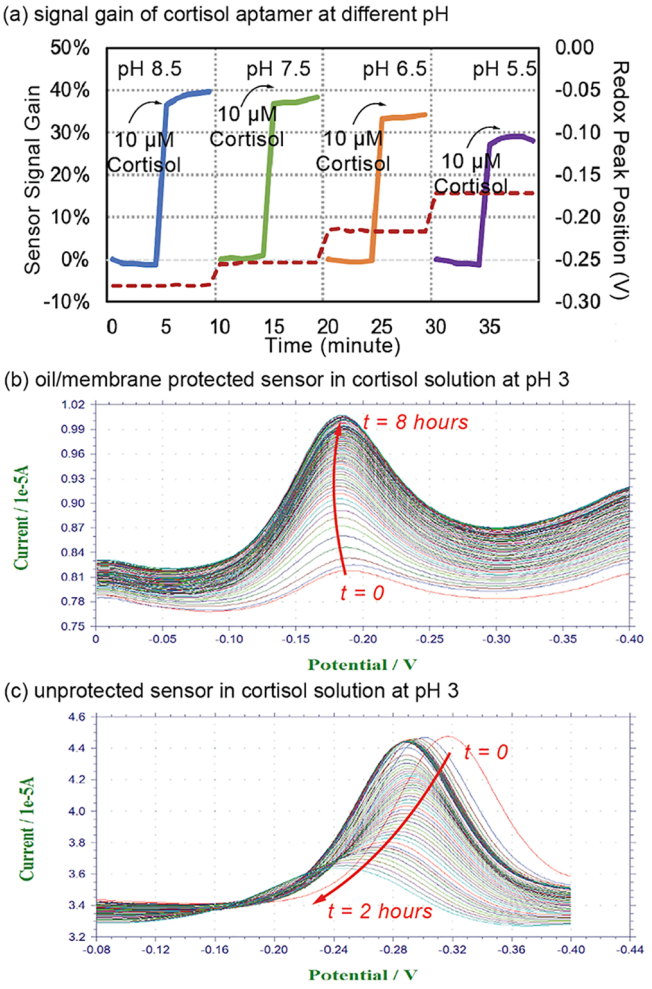

Figure 6. (a) EAB cortisol sensor in the solution with/without cortisol from pH 8.5 to 5.5. Sensor signal gain (solid lines) and redox couple peak position (dotted line). (b, c) Signal changes of EAB cortisol sensor using a U-boat setup (Figure 5a) with and without the oil membrane while testing in a 10 μM cortisol solution at pH = 3 for hours.

Initially, on the basis of the results in the previous sections, the three best-performing oils (1-decanol, castor oil, and tetradecane) are chosen for the fully integrated device tests. However, tetradecane is not compatible with the epoxy used to assemble the sensor, nor does it remain stably wetted in the membrane pores (the interfacial tension being potentially too large with respect to the polycarbonate). As a result, Figure 7 only presents the data for castor oil and 1-decanol.

First, we will discuss the device concentration-on response time shown in Figure 7. As discussed in the Theoretical Basis and Device Design section, the cortisol diffusion time through the membrane and the resulting device on/off lag time should be affected by both K and viscosity. We do not have established information or experiment data on the K value of castor and 1-decanol in relation to cortisol. However, we can proportionally estimate them on the basis of the LogK(octanol/water) value of castor oil, 1-decanol, and cortisol. Castor oil has a higher LogK(octanol/water) value, which makes it more hydrophobic. The LogK(octanol/water) of 1-decanol is lower but closer to the LogK(octanol/water) value of cortisol than that of castor oil, which means that cortisol is more likely to easily diffuse in and out of 1-decanol as opposed to castor oil that may sequester cortisol within the oil membrane. At the same time, castor oil is 50× more viscous than 1-decanol (Table 1). The expected slower response time for castor-oil-membrane sealed sensor is reflected in Figure 7, where it takes more than 30 min for the signal to reach 90% of its plateau to a 10 μM cortisol change for the concentration-on process,

https://doi.org/10.1021/acsami.1c14175
ACS Appl. Mater. Interfaces XXXX, XXX, XXX−XXX

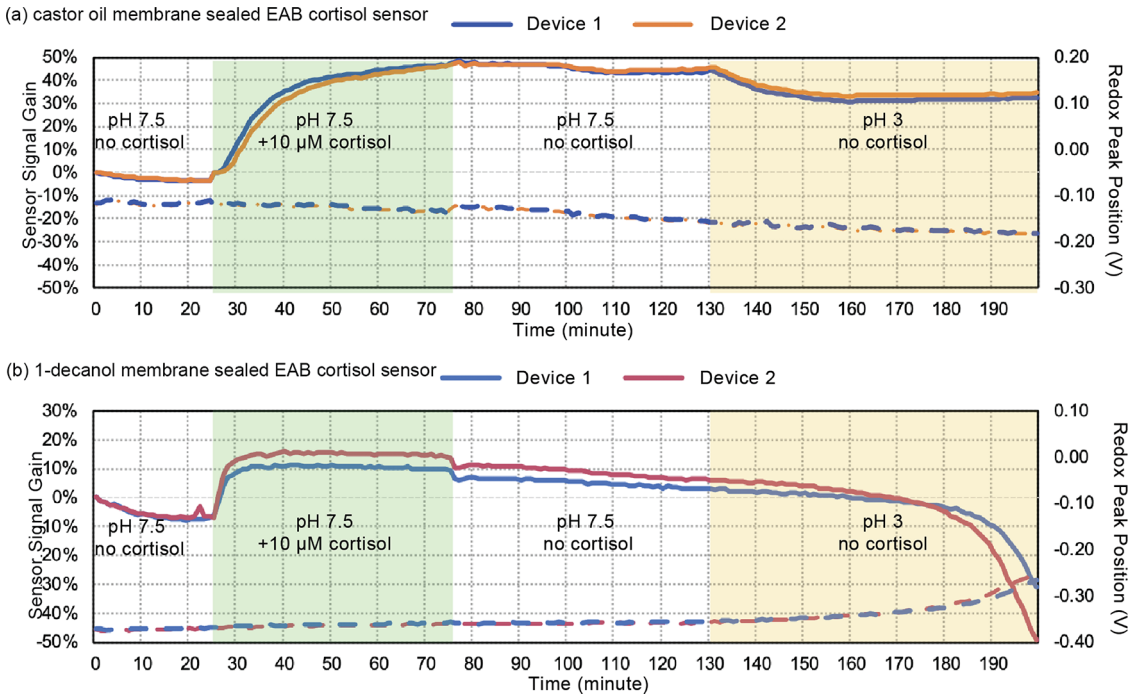

Figure 7. Response of EAB cortisol sensors (two tests per data set) with oil membranes fabricated with (a) castor oil and (b) 1-decanol. The plots contain both the sensor signal gain (solid line) and the redox peak position (dashed line) in different testing environments.

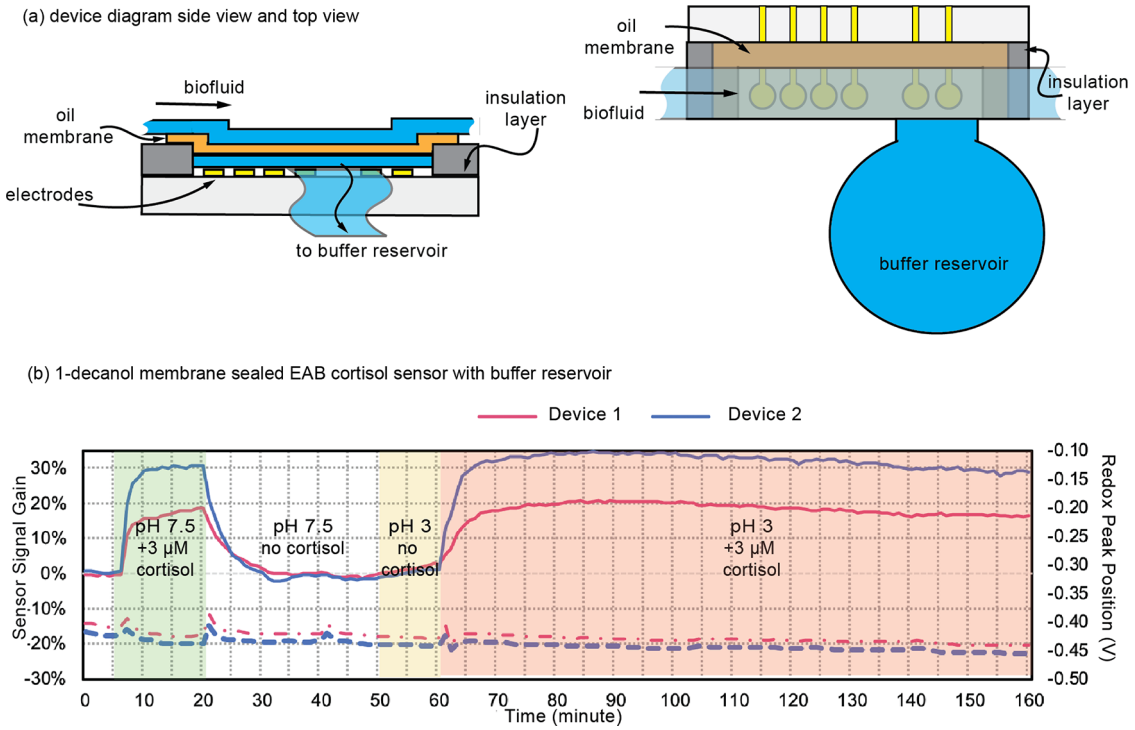

Figure 8. (a) Diagram of side/top view of the oil-membrane sealed EAB cortisol sensor with a buffer reservoir. (b) Improved performance on signal gain (solid line) and peak position (dashed line) from 1-decanol membrane protected EAB cortisol sensors with the addition of a buffer reservoir when diffusing different sample solutions over the oil membrane.

while it takes less than 5 min for the 1-decanol-membrane sealed sensor.

Next, we discuss the device concentration-off response time. As shown in Figure 7, for both castor oil and 1-decanol, the response to decreasing cortisol concentration is much slower and arguably unmeasurable compared to the declining signal as a result of the gradual sensor degradation over time. At this time, the absence of an off response is speculated to be due to retention in the oil, as discussed in the Theoretical Basis and Device Design section. It should be noted that we also test a well-stirred approach for the biofluid that should increase the diffusion-promoting concentration gradient at the oil membrane/biofluid interface; however, we do not see any improvements in the concentration-off time.

https://doi.org/10.1021/acsami.1c14175
ACS Appl. Mater. Interfaces XXXX, XXX, XXX−XXX

Lastly, to confirm that each test uses an oil membrane with high integrity (no leaks) and to test the ability of the oil membrane to protect against pH, our final step in the experiments in Figure 7 is to place the device in a solution of pH 3 and no cortisol content. A pH 3 solution is an extreme testing environment—beyond what is needed for pH variability in most biofluids—but has been tested here to quickly reveal any failure of the oil-membrane protection. As shown in Figure 7, only small changes in the redox peak position are observed for the castor-oil-membrane sealed sensor; in contrast, for the 1-decanol-membrane sealed sensor, the signal gain starts to decrease, while the redox peak position simultaneously shifts toward a more positive potential after 40 min. According to the results from the disk sensor test, this shift in redox potential indicates that the sensing solution is becoming more acidic. In other words, charged pH-influencing molecules are partitioning through the oil membrane containing 1-decanol, likely due to its lower K value and viscosity compared to castor oil. One last observation based on the data of Figure 7 is that, for the castor oil test group, the redox peak does not shift toward a more positive potential, but there is a slow gradual negative potential shift. It is speculated that this could be due to castor oil having a slight water solubility and high molecular heterogeneity. As a result, the hydrophobic tails of castor oil could result in fouling the surface of the gold electrodes. This would result in greater electrical resistance and, therefore, greater potential to generate the redox peak.

Stronger Buffer to Improve pH Protection. With 1-decanol as the highest-performing oil in terms of a fast concentration-on time but also with reduced protection to pH, a simple solution to improve pH protection is next explored. Simply, the solution on the sensor side is more strongly buffered. We enhance the buffer capacity of our SSS sensor solution by adding PBS powder to a final concentration of either 1× PBS or 33× PBS. Results shown in Figure S2 are the SSS/1× PBS solution and SSS/33× PBS solution on the sensor side of the oil membrane. A higher buffer capacity notably increases the device longevity for both buffer conditions compared to no additional buffer. The redox peak position of the sensor with the 1× buffer capacity holds for 140 min when exposed to an acidic environment and 440 min for the sensor with the 33× buffer capacity. Importantly, the lag time for cortisol diffusing through the oil membrane remains between 5 and 7 min. A doubled signal gain is observed from the sensor with the 33× buffer capacity. However, with our hand-fabricated sensors, we regularly see variations between the sensors in their signal gain. At 33× buffer capacity, the NaCl concentration is about 4.6 M, supporting our earlier claim that our EAB cortisol sensor operates robustly even in high-salt conditions.

An Additional Buffer Reservoir Resolves Concentration-Off Challenges and Buffering Capacity. Our final redesign of the device pursued in this work is arguably the most compelling from an application perspective, as it resolves both the longevity concerns of the sensor system as well as the concentration-off response-time challenges both discussed theoretically and shown experimentally in previous sections. As shown in Figure 8, a buffer reservoir containing 1× PBS is added with a diffusion-limited connection to the sensor solution side of the oil membrane. In Figure 8, a constant flow of biofluid is also provided for the first time in this work. The addition of the buffer reservoir has two purposes. First, the buffer reservoir is able to constantly diffuse in the additional buffer to mitigate any change in pH due to the biofluid. This simply requires that the buffer reservoir pathway for the additional buffer is less resistant to the diffusion of the buffer than the diffusion of acids and bases through the oil membrane pathway (this is easily achievable). Second, the buffer reservoir provides another diffusion pathway to continuously remove the analyte, theoretically resulting in a faster concentration-off response. The experimental results shown in Figure 8 fully support this expected behavior. By adding the buffer reservoir, the concentration-off process is greatly quickened: the concentration-off time is reduced to 10 min at 90% of signal off. Furthermore, there appears to be no limitation on the buffer capacity even in the highly challenging test at pH 3 for the biofluid. It should be noted that the concentration-on process is slowed to about 10 min for 90% signal on. This is not unexpected given that a constant flow of biofluid approach is used in Figure 8 and because the buffer reservoir is constantly removing cortisol. Although the approach in Figure 8 is unoptimized in this work, the addition of a buffer reservoir is an elegant and simple solution to observed challenges in both buffer capacity and concentration-off response time. Thinner 3 μm membranes with uniform porosity are also attempted, which increase the oil/water interface by ∼10× (Figure S6).

CONCLUSIONS

In this work, we demonstrate the efficacy of an oil-membrane sensor protection approach, including its design and operation with cortisol analyte in both the presence and absence of interferents. Although the cortisol aptamer sensor results can be highly variable from sensor-to-sensor in terms of signal gain, the effects of oil-membrane protection are consistent and clear across all the figures. Furthermore, the cortisol sensor variability can be corrected for using kinetic differential measurement techniques.[33,34] The results demonstrate the basic feasibility of the oil-membrane approach for sensor protection and do so over time scales (>3 h) and response time (1s to 10s of minutes) that are relevant for both point-of-care and continuous biosensing applications. We propose that the buffer-reservoir approach of Figure 8 is the preferred approach for continuous biosensing given its ability to allow the sensor to respond to both increases and decreases in cortisol concentration, as well as to provide buffering of the sensor for prolonged periods. Although only cortisol is demonstrated in this work, a rapid oil optimization can be implemented for each new analyte, as was shown in Figure 4. Furthermore, although not explored here, we speculate that future work would focus on two or three oil systems with vastly different hydrophobicity but that are miscible and therefore can be mixed to provide an ideal K for any particular analyte and application.

METHODS

Materials. All oils, reagents, and cortisol solution were purchased from Sigma-Aldrich (St. Louis, MO). The 96 transwell plate was purchased from Sigma-Aldrich (St. Louis, MO). The polycarbonate track-etch membrane with a 1 μm diameter pore size was obtained from Sterlitech Corporation (Kent, WA). The cortisol aptamer solution and synthetic sweat solution were obtained from Eccrine Systems, Inc. (Cincinnati, OH). The titration curve for the cortisol aptamer is provided in Figure S7. The cortisol aptamer, like other small molecule aptamers, does not require regeneration (inherently fast on and off response times). Samples of adhesive materials Crystal-clear Gorilla Tape, Kapton polyimide double-sided tape, and marine epoxy were purchased from Amazon (Seattle, CA). The acrylic was purchased from McMaster-Carr (Princeton, NJ).

Sensor Functionalization. The gold planar electrodes were manufactured using a Temescal FC-1800 E-Beam Evaporator from Ferrotec (CA, USA). Ti (40 nm thick) was deposited on the glass slide as an adhesion promoting layer prior to the 200 nm gold layer. A layer of Kapton polyimide film, laser cut to size (geometric design shown in Figure 3), was applied on top of the glass substrate.

For cleaning, the electrode array was connected to a CHI E600 electrochemical analyzer through 5252 SOIC clips from Pomona Electronics (CA, USA). Each foot was connected to an individual working channel. A Pt wire electrode and a Ag/AgCl electrode were wired as a common counter electrode and common reference electrode, respectively, shared by six channels. The electrode array was immersed in a 0.5 M H_2SO_4 solution. Cyclic voltammetry was applied to a 1 V/s scan rate from 0 to 1.6 V to electrochemically clean the surface of the electrode. The surface was rinsed with DI water and

https://doi.org/10.1021/acsami.1c14175
ACS Appl. Mater. Interfaces XXXX, XXX, XXX−XXX

dried under an air gun. This was followed by O_2 plasma cleaning for 2 min.

A 400 nM cortisol aptamer solution was drop casted onto the surface of working electrodes and allowed to incubate in the dark for an hour. The cortisol aptamer was obtained from Eccrine Systems, Inc. (Cincinnati, OH). The remaining solution was shaken off after incubation. Then a 5 mM mercaptohexanol (MCH) solution from Sigma-Aldrich (St. Louis, MO) was used to further passivate the surface of the working, counter, and reference electrodes. The functionalized electrodes were stored in a dry hood for 2 h and protected from the light. When this process was completed, the surface was rinsed with DI water to get rid of the extra MCH.

The gold rod electrode was purchased from CH Instruments, Inc. (Austin, TX). The cleaning and functionalization process were the same as those of the planar electrodes.

Integration for the Device without a Buffer Reservoir. The oil-membrane device shown in Figure 2 includes four subassemblies: the sensor substrate, the top adhesive assembly, the bottom adhesive assembly, and the membrane. The membrane was cut to fit the 15 × 2 mm operation window. The bottom adhesive component was composed of a layer of Crystal-clear Gorilla Tape and a layer of Kapton polyimide double-sided tape. The top adhesive was a layer of Kapton polyimide double-sided tape attached to a 1.25 mm thick acrylic. Both adhesive components were laser cut into a 20 × 4 mm rectangle with a 15 × 2 mm open window. And the polycarbonate track-etch membrane was placed between the two adhesives with both sides facing the Kapton polyimide double-sided tape.

For assembly, we first placed the functionalized sensor into a 100 mm diameter petri dish filled with the PBS solution. With the oil-membrane and bottom- and top-adhesive assemblies all attached to each other, we then placed them onto the sensor electrode array. Once assembled, the device was removed from the solution, we dried the extra solution on its outside, and the device was quickly sealed with the Brampton marine epoxy from Brampton Technology Ltd. (CT, USA) along the perimeter of the device. After 30 min and once the epoxy was cured, the sensor was ready for testing.

Integration for the Device with a Buffer Reservoir. In Figure 8, the sensor electrode array was connected to 5252 SOIC clips from Pomona Electronics (CA, USA) and placed flat. A 10 cm diameter petri dish was filled with 1× PBS solution and placed right next to the sensor as a buffer reservoir. A 5 mm wide L-shape cutout of a single layer of Kimtech Science Kimwipes Delicate Task Wipe was fully saturated with the PBS solution. One 5 mm long leg of the L-shape Kimwipes tissue was applied onto the sensor. The other leg was connected to the buffer reservoir. A layer of polycarbonate track-etch membrane saturated with oil was applied on top of the Kimwipes tissue. A 5 mm wide strip was cut out from a single layer of Kimtech Science Kimwipes Delicate Task Wipe, wetted with the buffer solution, and applied on top to pass the sample solution from a syringe pump over the oil membrane to a waste pump. The sample solution was pumped at 4 μL/min. A 5 × 5 × 3 mm acrylic block was then placed on top of the strip as a weight to hold all the layers compressed against each other. A labeled photograph of this device is provided with the online supplementary material for this article (Figure S3).

Data Generation and Analysis. During the test, the sensor was connected to a CHI E600 (CH Instruments, Inc., Austin, TX) through 5252 SOIC clips. Square wave voltammetry was used within a scanning window of 0 to −0.5 V, with an amplitude of 0.035 V and a frequency of 500 Hz (for rod electrodes) or 120 Hz (for planar electrodes). The raw data were exported from a saved text file from the CH Instrument (Austin, TX) Software. The signals were processed by a customized model in MATLAB (available at https://www.mathworks.com/products/matlab.html). The signal gain was measured by reading the highest current within two manually set potential points and then subtracting the baseline linearly matched by these two set points.

■ ASSOCIATED CONTENT

Supporting Information

The Supporting Information is available free of charge at https://pubs.acs.org/doi/10.1021/acsami.1c14175.

Polycarbonate track-etch membrane properties; equivalent diffusion distance calculation for castor oil and 1-decanol soaked membrane; sensor response at different salinity levels; 1-decanol membrane sealed sensor with 1× and 33× buffer capacity response for 10 h; picture of the experiment setup for the device connected with a buffer reservoir; 1-decanol membrane sealed sensor response with different flow rates; additional tests for 1-decanol membrane sealed sensor; cortisol aptamer titration curve in PBS and in serum; and sensor performance in PBS with 1-decanol oil-membrane protection against serum over 12 h (PDF)

■ AUTHOR INFORMATION

Corresponding Author

Jason Heikenfeld − *Novel Devices Lab, University of Cincinnati, Cincinnati, Ohio 45221, United States;* orcid.org/0000-0001-5778-8343; Email: heikenjc@ucmail.uc.edu

Authors

Yuchan Yuan − *Novel Devices Lab, University of Cincinnati, Cincinnati, Ohio 45221, United States*

Madeleine DeBrosse − *Novel Devices Lab, University of Cincinnati, Cincinnati, Ohio 45221, United States; 711 Human Performance Wing, Air Force Research Laboratory, Wright-Patterson AFB, Ohio 45433, United States*

Michael Brothers − *711 Human Performance Wing, Air Force Research Laboratory, Wright-Patterson AFB, Ohio 45433, United States;* orcid.org/0000-0002-8239-2399

Steve Kim − *711 Human Performance Wing, Air Force Research Laboratory, Wright-Patterson AFB, Ohio 45433, United States;* orcid.org/0000-0002-9519-077X

Alexandra Sereda − *PMI R&D, Philip Morris Products SA, 2000 Neuchâtel, Switzerland*

Nikolai V. Ivanov − *PMI R&D, Philip Morris Products SA, 2000 Neuchâtel, Switzerland*

Saber Hussain − *711 Human Performance Wing, Air Force Research Laboratory, Wright-Patterson AFB, Ohio 45433, United States*

Complete contact information is available at: https://pubs.acs.org/10.1021/acsami.1c14175

Author Contributions

The manuscript was written and edited through contributions of all authors. All authors have given approval to the final version of the manuscript.

Notes

The authors declare the following competing financial interest(s): Corresponding author Jason Heikenfeld has an equity interest in Eccrine Systems, Inc., a company that may potentially benefit from the research results. The terms of this arrangement have been reviewed and approved by the University of Cincinnati in accordance with its conflict-of-interest policies. Alexandra Sereda and Nikolai V. Ivanov are employees of Philip Morris International.

https://doi.org/10.1021/acsami.1c14175
ACS Appl. Mater. Interfaces XXXX, XXX, XXX−XXX

■ ACKNOWLEDGMENTS

The work featured here spans multiple years of work and multiple affiliated research contracts and collaborators between the University of Cincinnati and the United States Air Force Research Laboratory. The authors acknowledge partial support from the National Science Foundation ECCS Award #1608275 and ECCS Award #2025720, DAGSI/SOCHE Award #RH1-UC-19-4, Air Force Research Labs (USAF Contract FA8650-16-C-6760), and the Ohio Federal Research Network (PO FY16-049 and WSARC-1077-700). The 711th Human Performance Wing authors acknowledge the Air Force Research Laboratory for funding as well as the Oak Ridge Institute for Science and Education (ORISE) for partial funding. This work has also been supported in part by Philip Morris International.

■ ABBREVIATIONS

EAB, electrochemical aptamer-based
NAD+/NADH, nicotinamide adenine dinucleotide/reduced nicotinamide adenine dinucleotide
FAD/FADH2, flavin adenine dinucleotide/reduced flavin adenine dinucleotide
PBS, phosphate-buffered saline
ELISA, enzyme-linked immunosorbent assay
DI, distilled water
SSS, synthetic sweat solution
MCH, 6-mercapto-1-hexanol

■ REFERENCES

(1) Shah, V. N.; Laffel, L. M.; Wadwa, R. P.; Garg, S. K. Performance of a Factory-Calibrated Real-Time Continuous Glucose Monitoring System Utilizing an Automated Sensor Applicator. *Diabetes Technol. Ther.* **2018**, *20*, 428−433.
(2) Rocchitta, G.; Spanu, A.; Babudieri, S.; Latte, G.; Madeddu, G.; Galleri, G.; Nuvoli, S.; Bagella, P.; Demartis, M. I.; Fiore, V.; Manetti, R.; Serra, P. A. Enzyme Biosensors for Biomedical Applications: Strategies for Safeguarding Analytical Performances in Biological Fluids. *Sensor* **2016**, *16*, 780.
(3) Heikenfeld, J.; Jajack, A.; Feldman, B.; Granger, S. W.; Gaitonde, S.; Begtrup, G.; Katchman, B. A. Accessing Analytes in Biofluids for Peripheral Biochemical Monitoring. *Nat. Biotechnol.* **2019**, *37*, 407−419.
(4) Hianik, T.; Ostatná, V.; Sonlajtnerova, M.; Grman, I. Influence of Ionic Strength, PH and Aptamer Configuration for Binding Affinity to Thrombin. *Bioelectrochemistry* **2007**, *70*, 127−133.
(5) Park, C.; Raines, R. T. Quantitative Analysis of the Effect of Salt Concentration on Enzymatic Catalysis. *J. Am. Chem. Soc.* **2001**, *123*, 11472−11479.
(6) Xiao, Y.; Lubin, A. A.; Heeger, A. J.; Plaxco, K. W. Label-Free Electronic Detection of Thrombin in Blood Serum by Using an Aptamer-Based Sensor. *Angew. Chem., Int. Ed.* **2005**, *44*, 5456−5459.
(7) Brothers, M. C.; DeBrosse, M.; Grigsby, C. C.; Naik, R. R.; Hussain, S. M.; Heikenfeld, J.; Kim, S. S. Achievements and Challenges for Real-Time Sensing of Analytes in Sweat within Wearable Platforms. *Acc. Chem. Res.* **2019**, *52*, 297−306.
(8) Arroyo-Currás, N.; Dauphin-Ducharme, P.; Scida, K.; Chávez, J. L. From the Beaker to the Body: Translational Challenges for Electrochemical Aptamer-Based Sensors. *Anal. Methods* **2020**, *12*, 1288−1310.
(9) De Bolle, X.; Vinals, C.; Fastrez, J.; Feytmans, E. Bivalent Cations Stabilize Yeast Alcohol Dehydrogenase I. *Biochem. J.* **1997**, *323*, 409−413.) (Pt 2),
(10) Belleperche, M.; DeRosa, M. C. PH-Control in Aptamer-Based Diagnostics, Therapeutics, and Analytical Applications. *Pharmaceuticals* **2018**, *11*, 80.
(11) Jang, C.; Lee, H.-J.; Yook, J.-G. Radio-Frequency Biosensors for Real-Time and Continuous Glucose Detection. *Sensors* **2021**, *21*, 1843.
(12) Müsse, A.; La Malfa, F.; Brunetti, V.; Rizzi, F.; De Vittorio, M. Flexible Enzymatic Glucose Electrochemical Sensor Based on Polystyrene-Gold Electrodes. *Micromachines* **2021**, *12*, 805.
(13) Vadgama, P. Monitoring with In Vivo Electrochemical Sensors: Navigating the Complexities of Blood and Tissue Reactivity. *Sensors* **2020**, *20*, 3149.
(14) Schoukroun-Barnes, L. R.; Wagan, S.; Liu, J.; Leach, J. B.; White, R. J. Biocompatible Hydrogel Membranes for the Protection of RNA Aptamer-Based Electrochemical Sensors. In *Smart Biomedical and Physiological Sensor Technology X*; Cullum, B. M.; McLamore, E. S., Eds.; SPIE: 2013; Vol. *8719*, pp. 73−80, DOI: 10.1117/12.2016020.
(15) Sonner, Z.; Wilder, E.; Heikenfeld, J.; Kasting, G.; Beyette, F.; Swaile, D.; Sherman, F.; Joyce, J.; Hagen, J.; Kelley-Loughnane, N.; Naik, R. The Microfluidics of the Eccrine Sweat Gland, Including Biomarker Partitioning, Transport, and Biosensing Implications. *Biomicrofluidics* **2015**, *9*, No. 031301.
(16) Somerson, J.; Plaxco, K. W. Electrochemical Aptamer-Based Sensors for Rapid Point-of-Use Monitoring of the Mycotoxin Ochratoxin A Directly in a Food Stream. *Molecules* **2018**, *23*, 912.
(17) Bohnert, T.; Gan, L.-S. Plasma Protein Binding: From Discovery to Development. *J. Pharm. Sci.* **2013**, *102*, 2953−2994.
(18) Shinoda, W. Permeability across Lipid Membranes. *Biochim. Biophys. Acta, Biomembr.* **2016**, *1858*, 2254−2265.
(19) Menichetti, R.; Kanekal, K. H.; Bereau, T. Drug−Membrane Permeability across Chemical Space. *ACS Cent. Sci.* **2019**, *5*, 290−298.
(20) Bedrov, D.; Smith, G. D.; Davande, H.; Li, L. Passive Transport of C60 Fullerenes through a Lipid Membrane: A Molecular Dynamics Simulation Study. *J. Phys. Chem. B* **2008**, *112*, 2078−2084.
(21) National Center for Biotechnology Information *PubChem Compound Summary for CID 12389, Tetradecane*; https://pubchem.ncbi.nlm.nih.gov/compound/Tetradecane. Accessed Sept. 17, 2020.
(22) National Center for Biotechnology Information *PubChem Compound Summary for CID 14030006, Castor oil*; https://pubchem.ncbi.nlm.nih.gov/compound/Castor-oil. Accessed Sept. 17, 2020.
(23) National Center for Biotechnology Information *PubChem Compound Summary for CID 8174, 1-Decanol*; https://pubchem.ncbi.nlm.nih.gov/compound/1-Decanol. Accessed Sept. 17, 2020.
(24) National Center for Biotechnology Information *PubChem Compound Summary for CID 12399, Dioctyl ether*; https://pubchem.ncbi.nlm.nih.gov/compound/Dioctyl-ether. Accessed Sept. 17, 2020.
(25) National Center for Biotechnology Information *PubChem Compound Summary for CID 445639, Oleic acid*; https://pubchem.ncbi.nlm.nih.gov/compound/Oleic-acid. Accessed Sept. 17, 2020.
(26) National Center for Biotechnology Information *PubChem Compound Summary for CID 5284607, Vitamin K1*; https://pubchem.ncbi.nlm.nih.gov/compound/Vitamin-K1. Accessed Sept. 17, 2020.
(27) National Center for Biotechnology Information *PubChem Compound Summary for CID 8195, 1-Dodecanethiol*; https://pubchem.ncbi.nlm.nih.gov/compound/1-Dodecanethiol. Accessed Sept. 17, 2020.
(28) Rachmawati, H.; Arvin, Y. A.; Asyarie, S.; Anggadiredja, K.; Tjandrawinata, R. R.; Storm, G. Local Sustained Delivery of Bupivacaine HCl from a New Castor Oil-Based Nanoemulsion System. *Drug Deliv. Transl. Res.* **2018**, *8*, 515−524.
(29) Ogunniyi, D. S. Castor Oil: A Vital Industrial Raw Material. *Bioresour. Technol.* **2006**, *97*, 1086−1091.
(30) Behera, B.; Biswal, D.; Uvanesh, K.; Srivastava, A. K.; Bhattacharya, M. K.; Paramanik, K.; Pal, K. Modulating the Properties of Sunflower Oil Based Novel Emulgels Using Castor Oil Fatty Acid Ester: Prospects for Topical Antimicrobial Drug Delivery. *Colloids Surf., B* **2015**, *128*, 155−164.
(31) Bandodkar, A. J.; Hung, V. W. S.; Jia, W.; Valdés-Ramírez, G.; Windmiller, J. R.; Martinez, A. G.; Ramírez, J.; Chan, G.; Kerman, K.;

https://doi.org/10.1021/acsami.1c14175
ACS Appl. Mater. Interfaces XXXX, XXX, XXX−XXX

Wang, J. Tattoo-Based Potentiometric Ion-Selective Sensors for Epidermal PH Monitoring. *Analyst* **2013**, *138*, 123−128.
(32) Baliga, S.; Muglikar, S.; Kale, R. Salivary PH: A Diagnostic Biomarker. *J. Indian Soc. Periodontol.* **2013**, *17*, 461−465.
(33) Ferguson, B. S.; Hoggarth, D. A.; Maliniak, D.; Ploense, K.; White, R. J.; Woodward, N.; Hsieh, K.; Bonham, A. J.; Eisenstein, M.; Kippin, T. E.; Plaxco, K. W.; Soh, H. T. Real-Time, Aptamer-Based Tracking of Circulating Therapeutic Agents in Living Animals. *Sci. Transl. Med.* **2013**, *5*, 213ra165−213ra165.
(34) Arroyo-Currás, N.; Somerson, J.; Vieira, P. A.; Ploense, K. L.; Kippin, T. E.; Plaxco, K. W. Real-Time Measurement of Small Molecules Directly in Awake, Ambulatory Animals. *Proc. Natl. Acad. Sci.* **2017**, *114*, 645.

https://doi.org/10.1021/acsami.1c14175
ACS Appl. Mater. Interfaces XXXX, XXX, XXX−XXX